# Crystal structure of a platelet-agglutinating factor isolated from the venom of Taiwan habu (*Trimeresurus mucrosquamatus*)

Kai-Fa HUANG*†, Tzu-Ping KO*, Chin-Chun HUNG*, John CHU*, Andrew H.-J. WANG*†[1] and Shyh-Horng CHIOU*†[1]

*Institute of Biological Chemistry, Academia Sinica, Nankang, Taipei 11529, Taiwan, and †Institute of Biochemical Sciences, National Taiwan University, Taipei 106, Taiwan

Platelet glycoprotein Ib (GPIb)-binding proteins (GPIb-BPs) from snake venoms are usually C-type lectins, which target specific sites of GPIb$\alpha$ and elicit distinct effects on platelets. In the present paper, we report a tetrameric platelet-agglutinating factor (molecular mass 121.1 kDa), termed mucrocetin, purified from the venom of Taiwan habu (*Trimeresurus mucrosquamatus*). Mucrocetin is a GPIb$\alpha$ agonist with a binding site distinct from that of flavocetin-A (a snake venom GPIb$\alpha$ antagonist) on GPIb$\alpha$, in spite of the high sequence identity (94.6 %) between the two venom lectins. The crystal structure of mucrocetin was solved and refined to 2.8 Å (1 Å = 0.1 nm) resolution, which shows an interesting crystal packing of six-layer cylinders of doughnut-shaped molecules. The four $\alpha\beta$ heterodimers are arranged in an unusual square-shaped ring stabilized by four interdimer 'head-to-tail' disulphide bridges. Detailed structural comparison between mucrocetin and flavocetin-A suggests that their disparate platelet effects are probably attributable to different charge distributions on the putative concave binding surface. A unique positively charged patch on the binding surface of mucrocetin, formed by $Lys^{102}$, $Lys^{108}$, $Lys^{109}$ and $Arg^{123}$ in the $\alpha$-subunit coupled with $Lys^{22}$, $Lys^{102}$, $Lys^{116}$ and $Arg^{117}$ in the $\beta$-subunit, appears to be the primary determinant of its platelet-agglutinating activity. Conceivably, this interesting venom factor may provide a useful tool to study platelet agglutination by binding to the GPIb–IX–V complex.

Key words: flavocetin-A, lectin-like protein, mucrocetin, platelet glycoprotein Ib, snake venom, *Trimeresurus mucrosquamatus*.

## INTRODUCTION

The interaction of von Willebrand factor (vWf) A1 domain with the platelet glycoprotein Ib$\alpha$ (GPIb$\alpha$) is important in mediating the initial tethering and rolling of platelets on the subendothelium of injured vessel walls [1,2]. Several exogenous modulators, such as ristocetin and some venom proteins [3–5], were shown to promote the formation of vWf–GPIb$\alpha$ complex through the binding to the A1 (or A3) domain of vWf. In addition, a number of GPIb-binding proteins (GPIb-BPs) were found in the venoms of many crotalid and viperid snakes [6,7], which either play the role of GPIb antagonist to block the binding of vWf to GPIb$\alpha$ or behave as GPIb agonists to induce platelet aggregation or agglutination.

Up to now, several venom GPIb$\alpha$ antagonists and their full-length sequences have been reported (summarized in Table 1) [8–13]. These venom proteins, with the exception of flavocetin-A (FL-A), exist as $\alpha\beta$ heterodimers of approx. 27 kDa, with the two subunits being approx. 14 kDa and 15 kDa. In contrast, FL-A is a tetrameric form of $\alpha\beta$ heterodimers linked by four interdimer cysteine bridges [14]. These venom factors block ristocetin- or botrocetin-induced aggregation of platelet-rich plasma (PRP), but they had no effect on ADP-induced aggregation. On the other hand, alboaggregin A and B and agglucetin are venom GPIb$\alpha$ agonists (Table 1), capable of directly inducing aggregation or agglutination of washed or fixed human platelets [15,16]. Alboaggregin A and agglucetin were reported to exist in high-molecular-mass forms of approx. 50 kDa, composed of disulphide-linked $\alpha$, $\beta$, $\gamma$ and $\delta$ (or $\alpha1$, $\alpha2$, $\beta1$ and $\beta2$ in agglucetin) subunits, whereas alboaggregin B is an $\alpha\beta$ heterodimer. The tetrameric alboaggregin A is stronger in terms of inducing platelet aggregation and subsequent release reaction than alboaggregin B [15]. Although these GPIb-BPs are structurally similar and target on the same platelet receptor, they appeared to bind to distinct or partially overlapping sites on GPIb$\alpha$ [10].

Crystal structures of the similar lectin-like venom proteins showed that the $\alpha$ and $\beta$ subunits are dimerized by domain swapping, creating a central concave surface, which could be important as a binding site for the target molecules [14,17]. The projected loop and the adjoining subunit complete the C-type carbohydrate-recognition domain (CRD) fold. However, they generate a large conformational change on the hinge region classically involved in $Ca^{2+}$- and carbohydrate-binding, resulting in the disruption of the lectin active site and the loss of carbohydrate-recognizing activity. The work of Mizuno et al. [18] on the elucidation of the complex structure between Factor X-binding protein and the $\gamma$-carboxyglutamic acid (Gla) domain of Factor X demonstrated that the concave surface is indeed the binding site for the Gla domain [18]. Close structural comparisons suggested that the determinants of lectin-like venom proteins for target recognition may reside on this concave surface, which has different surface charge potentials among various venom proteins [19].

In the present paper, the crystal structure and biological activity of a platelet-agglutinating factor, mucrocetin, purified from the venom of Taiwan habu (*Trimeresurus mucrosquamatus*) are reported. We found that mucrocetin shows a highly similar three-dimensional structure and a high sequence identity with that of FL-A. Surprisingly, further analysis of platelet-agglutinating activity suggested that mucrocetin is a GPIb$\alpha$ agonist with a binding site distinct from that of FL-A on GPIb$\alpha$. Since the binding sites of

Abbreviations used: CRD, carbohydrate-recognition domain; FL-A, flavocetin-A; GPIb, glycoprotein Ib; GPIb-BP, GPIb-binding protein; mAb, monoclonal antibody; NCS, non-crystallographic symmetry; PRP, platelet-rich plasma; r.m.s.d., root mean square deviation; vWf, von Willebrand factor.

[1] To whom correspondence should be addressed (e-mail ahjwang@gate.sinica.edu.tw or shchiou@gate.sinica.edu.tw).

The nucleotide sequences for the mucrocetin $\alpha$- and $\beta$-subunits have been deposited in the DDBJ, EMBL, GenBank® and GSDB Nucleotide Sequence Databases under the accession numbers AY390533 and AY390534 respectively. The atomic co-ordinates of the mucrocetin structure have been deposited at Research Collaboratory for Structural Bioinformatics (RCSB) Protein Data Bank under the accession number 1V4L.

**Table 1 Comparison of various platelet GPIb$\alpha$-targeting venom proteins**

| Venom protein and source | Subunit structure | Extra disulphide bridges for oligomerization | Action | MAbs with similar or adjacent binding sites on GPIb$\alpha$ |
|---|---|---|---|---|
| Flavocetin A (*Trimeresurus flavoviridus*) [14] | $(\alpha\beta)_4$ | Yes | Antagonist | GUR83–35† |
| Echicetin (*Echis carinatus*) [8] | $\alpha\beta$ | No | Antagonist | AK2 and SZ2 |
| Agkicetin-C (*Agkistrodon acutus*) [9] | $\alpha\beta$ | No | Antagonist | AK2 |
| *Jararaca* GPIb-BP (*Bothrops jararaca*) [11] | $\alpha\beta$ | No | Antagonist | AP1 |
| Mamushigin (*Agkistrodon halys blomhoffi*) [12] | $\alpha\beta$ | No | Antagonist | AP1 |
| CHH-B (*Crotalus horridus horridus*) [10] | $\alpha\beta$ | No | Antagonist | AK2 |
| Alboaggregin A (*Trimeresurus albolabris*) [15] | $\alpha\beta\delta\gamma$ | Yes | Agonist | AK2 and SZ2 (adjacent)‡ |
| Alboaggregin B (*Trimeresurus albolabris*) [15] | $\alpha\beta$ | No | Agonist | AK2 and SZ2 |
| Agglucetin (*Agkistrodon acutus*) [16] | $\alpha_1\alpha_2\beta_1\beta_2$ | Yes | Agonist | AP1 and LJ-Ib1 |
| Mucrocetin (*Trimeresurus mucrosquamatus*) | $(\alpha\beta)_4$ | Yes | Agonist | CD42b Ab-1§ |

† Targeting sites of these mAbs on platelet GPIb are as follows: GUR83-35 and LJ-Ib1, within $His^1$–$Arg^{293}$ of GPIb$\alpha$; AK2, $Leu^{36}$–$Gln^{59}$; SZ2, $Tyr^{276}$–$Glu^{282}$; AP1, $Phe^{201}$–$Gly^{268}$.
‡ Alboaggregin A, performed in a cross-blocking study [10], strongly blocked AK2 and only partially blocked SZ2 binding to GPIb$\alpha$.
§ mAb was produced by using both GPIb$\alpha$- and $\beta$-chain as antigen.

lectin-like venom proteins on GPIb$\alpha$ are not congruent, mucrocetin may offer an elegant case in probing the structural basis of snake venom GPIb-BPs for the binding and activation of GPIb$\alpha$.

## MATERIALS AND METHODS

### Reagents

The crude venoms of *T. mucrosquamatus* were obtained from a local snake farm, and the venom glands were kindly provided by the National Institute of Preventive Medicine, Taipei, Taiwan. Freeze-dried venom of *Trimeresurus flavoviridis* was purchased from Sigma Chemical Co. (St. Louis, MO, U.S.A.). TSK DEAE-650 anion-exchange resin was obtained from Merck KGaA (Darmstadt, Germany). Sephadex G-100 and Q Sepharose resins, the QuickPrep™ mRNA preparation kit, and the cDNA Synthesis System Plus Kit were obtained from Amersham Biosciences (Uppsala, Sweden). Monoclonal antibody (mAb) CD42b Ab-1 (raised against the platelet GPIb) was purchased from Lab Vision Co. (Fremont, CA, U.S.A.). Ristocetin was obtained from Chrono-Log Co. (Havertown, PA, U.S.A.). All other reagents were purchased from either Sigma or Merck.

### Isolation and purification of mucrocetin and FL-A

Venom components were separated by anion-exchange chromatography on an open column (2.5 cm × 46 cm) packed with TSK DEAE-650 (M) gel suspension. Approx. 350 mg of venom powder was dissolved in 8 ml of starting buffer (0.025 M ammonium bicarbonate, pH 7.7) and applied to the column equilibrated with the same buffer. The column was extensively washed with starting buffer and was then eluted in a linear gradient of 0.025–0.5 M ammonium bicarbonate, pH 7.7, followed by 0.5–1.0 M ammonium bicarbonate, pH 8.0, similar to the method described previously [20]. A gel-filtration chromatographic step was carried out on a Sephadex G-100 (S) (1.6 cm × 120 cm) column, using 0.025 M ammonium bicarbonate at pH 7.8 as the elution buffer. Finally, a HPLC gel-filtration column (Bio-Sil SEC 250-5, 7.8 mm × 300 mm, Bio-Rad) on a Hitachi liquid chromatograph equipped with a model L-6200 pump and a tunable UV detector was used to purify further the fractions isolated from the above chromatographic steps.

We also purified FL-A according to the method reported by Taniuchi et al. [21] with some modifications. The purified proteins of FL-A were confirmed by platelet assays, N-terminal sequencing and immunoblotting analysis.

### Platelet-agglutination assay

Human peripheral blood collected from a healthy volunteer was anticoagulated with 0.1 vol. of sodium citrate (3.8 %, w/v). In order to prepare human PRP, the whole blood was centrifuged at 150 ***g*** for 12 min at room temperature (25 °C). Washed platelet suspension was prepared mainly according to the protocol described previously [22]. Isolated platelets were suspended in Tyrode's solution [0.1 % (w/v) glucose, 0.8 % (w/v) sodium chloride, 0.1 % (w/v) sodium bicarbonate, 0.02 % (w/v) potassium chloride, 0.005 % (w/v) sodium dihydrogen phosphate, 0.02 % (w/v) calcium chloride and 0.01 % (w/v) magnesium chloride, pH 7.4] and the platelet count was adjusted to $3–5 \times 10^8$ platelets/ml. Platelet agglutination was performed using an aggregometer (Chrono-Log) at 37 °C with stirring (1000 rev./min). The extent of platelet agglutination was monitored continuously for 10 min by turbidimetry and expressed as an increase in light transmission.

### Reduction, pyridylethylation and N-terminal sequence analysis of mucrocetin

Mucrocetin (approx. 2 nmol) was incubated in 100 $\mu$l of 0.25 M Tris/HCl, pH 8.5, containing 6 M guanidine hydrochloride, 1 mM EDTA and 5 % (v/v) 2-mercaptoethanol for 16 h at room temperature. Subsequently, 5 $\mu$l of 4-vinylpyridine was added and the incubation was continued for an additional 90 min. After acidification with pure formic acid, S-pyridylethylated subunits were separated and purified by RP-HPLC using a Vydac Protein C4 column (1 cm × 25 cm). The eluted mucrocetin subunits were freeze-dried and dissolved in 0.1 % (v/v) trifluoroacetic acid, before N-terminal sequence analysis.

### Cloning of mucrocetin cDNA

To prepare the cDNA mixture for PCR cloning, two deep-frozen venom glands from an individual snake were homogenized and polyadenylated RNAs were purified using the QuickPrep™ mRNA preparation kit. Double-stranded cDNA synthesis was carried out using the cDNA Synthesis System Plus Kit. For the cloning of mucrocetin cDNA, two oligonucleotide primers of sense and antisense orientations based on the highly conserved

5′- and 3′-non-coding regions of cDNAs coding for agkicetin-C [9] and mamushigin [12], with the forward sequence 5′-CTCTGCAGGGAAGGAAGGAAGACCATG-3′ and the reverse sequence 5′-TTGCTTCTCCAGACTTCAC(A/T)CAGC(C/T)G-3′, were synthesized. The reactions were subjected to 35 cycles of heat denaturation at 94 °C for 1.5 min, annealing the primers to the DNAs at 50 °C for 2 min, and DNA chain extension at 72 °C for 2.5 min, followed by a final extension at 72 °C for 10 min. The PCR products were subcloned into pGEM-T vector, and then transformed into *Escherichia coli* strain JM109. Plasmids purified from positive clones were prepared for nucleotide sequence analysis by automatic fluorescence-based sequencing using a model 373A DNA Sequencing System (Applied Biosystems, Foster City, CA, U.S.A.).

### Crystallization and data collection

Purified mucrocetin was concentrated to 52.3 mg/ml using an ultra-filtration membrane YM-30 (Millipore Amicon, Billerica, MA, U.S.A.). The screening for the crystals of mucrocetin was achieved using crystallization screening kits from Hampton Research (Laguna Niguel, CA, U.S.A.). Finally, mucrocetin in 0.025 M ammonium bicarbonate at pH 7.8 was mixed with an equal volume of the reservoir (2.5 M 1,6-hexanediol and 0.1 M sodium citrate at pH 5.6) and then crystallized at room temperature using the hanging-drop vapour-diffusion method. Crystals with their dimensions reaching 0.2 mm × 0.15 mm × 0.1 mm appeared within 1 week. X-ray diffraction data were first collected at Academia Sinica (Taipei, Taiwan) using MSC MicroMax-002 equipped with an R-AXIS IV$^{++}$ image-plate detector. Later, data were collected using beam line 41XU at SPring-8 (Hyogo, Japan) with a charge-coupled device (CCD) detector. Finally, more data were collected from beam line 17B2 at the National Synchrotron Radiation Research Center (Hsinchu, Taiwan) using a similar image-plate detector as above. Data were processed using the HKL package installed on Silicon Graphics Inc. (SGI) O2 workstations [23].

### Structure determination and refinement

For molecular replacement search, a 4.5 Å (1 Å = 0.1 nm) resolution data set collected using an in-house X-ray source and a tetrameric FL-A model generated from the PDB (Protein Data Bank) deposition 1C3A were employed. By the comparison of space group and unit cell dimension with those of FL-A, the mucrocetin crystal was estimated to contain three heterodimers in an asymmetric unit. By using the program CNS [24], three rotation function solutions were obtained, as expected, which corresponded to rotations of 62°, 78° and 93° about the 4-fold axis. A translation function search based on the three rotation function solutions also yielded three solutions, with the centres of tetramers remaining aligned with the *c*-axis and placed at 74.3 Å, 45.9 Å and 14.2 Å from the origin.

Preliminary refinement using the FL-A model while including strict non-crystallographic symmetry (NCS) constraints gave $R$ and $R_{free}$ values of 0.278 and 0.335 respectively, using the 3.3 Å data set collected at SPring-8. The resulting Fourier maps showed corresponding densities for most of the different amino-acid residues between FL-A and mucrocetin. Density modification with solvent flipping and 3-fold NCS averaging increased the overall figure of merit from 0.78 to 0.86, but the quality of the map was not significantly improved. Substitution of all amino-acid residues for the correct sequence of mucrocetin yielded $R$ and $R_{free}$ values of 0.282 and 0.312 respectively, after strict-NCS refinement. Subsequent cycles of refinement included manual adjustments of the protein model and addition of water molecules. Finally, further refinement by employing NCS restraints and using the synchrotron data from National Synchrotron Radiation Research Center was carried out. The final model of mucrocetin contains 601 water molecules located according to a density level of 1.2 $\sigma$ in the $2F_o$-$F_c$ maps.

## RESULTS

### Isolation and purification of mucrocetin and FL-A

*T. mucrosquamatus* venoms were separated on a TSK DEAE-650 anion-exchange column into at least 12 peaks (Figure 1), showing an elution pattern superior to that reported previously [20]. The fractions with strong platelet-agglutinating activity were collected. As judged by SDS/PAGE, a number of proteins in the pooled fraction showed molecular masses larger than 100 kDa under non-reducing conditions and distinct from the rest. Therefore further purification by Sephadex G-100 was carried out, which was followed by a final step of purification using a HPLC gel-permeation column to obtain pure mucrocetin. On SDS/PAGE, mucrocetin migrated as two distinct bands of 16 kDa and 14 kDa under reducing conditions, and a major band with an apparent molecular mass of 135 kDa under non-reducing condition (Figure 1, inset, lanes 2 and 4).

On the other hand, after purification, FL-A was analysed for the first five amino-acid residues of the two subunits. They are Asp-Phe-Asp-Xaa-Ile and Gly-Phe-Xaa-Xaa-Pro, in agreement with the $\alpha$- and $\beta$-chain of FL-A respectively [14]. The purified FL-A was also verified by its strong inhibitory activity on ristocetin-induced platelet aggregation in human PRP (Figure 2D). On SDS/PAGE, mucrocetin shows a similar mass to FL-A under non-reducing conditions (Figure 1, inset, lanes 3 and 4), while the $\alpha$-subunit of mucrocetin is slightly larger than that of FL-A under reducing conditions (Figure 1, inset, compare lanes 1 and 2). Rabbit antiserum raised against the $\alpha$-chain of mucrocetin significantly cross-interacted with the $\beta$-chain of mucrocetin (Figure 1, inset, lane 6), indicating the similar antigenicity between these two subunits of mucrocetin.

### Platelet-agglutination studies

Mucrocetin strongly induces platelet agglutination in either human PRP or washed platelet suspensions (Figure 2). It appears that mucrocetin agglutinates platelets in a vWf-independent manner, causing no obvious change of platelet shape. Similar agglutinating activities of mucrocetin in both PRP and washed platelets, with the maximum agglutination achieved at a concentration of approx. 2.5 $\mu$g/ml (18.5 nM), were observed (compare Figure 2A with Figure 2F), suggesting that mucrocetin does not modulate vWf as ristocetin and botrocetin do [3,4]. Moreover, mucrocetin pre-treatment had no effect on the aggregation of platelets induced by ristocetin (1.4 mg/ml) in human PRP (Figures 2B and 2C). Purified FL-A at 20 $\mu$g/ml, which is much higher than the reported $IC_{50}$ [21], completely abolished the aggregation induced by ristocetin in human PRP (Figure 2D), but it did not inhibit the mucrocetin-induced agglutinations in both PRP and washed platelets (Figures 2E and 2H). In addition, a mAb CD42b Ab-1, raised against the platelet GPIb, dose-dependently blocked the agglutination induced by mucrocetin with an $IC_{50}$ of 18.1 $\mu$g/ml (Figure 2G).

### N-terminal partial sequences of mucrocetin

Purified mucrocetins were reduced and S-pyridylethylated, and the dissociated subunits were separated using a reverse-phase

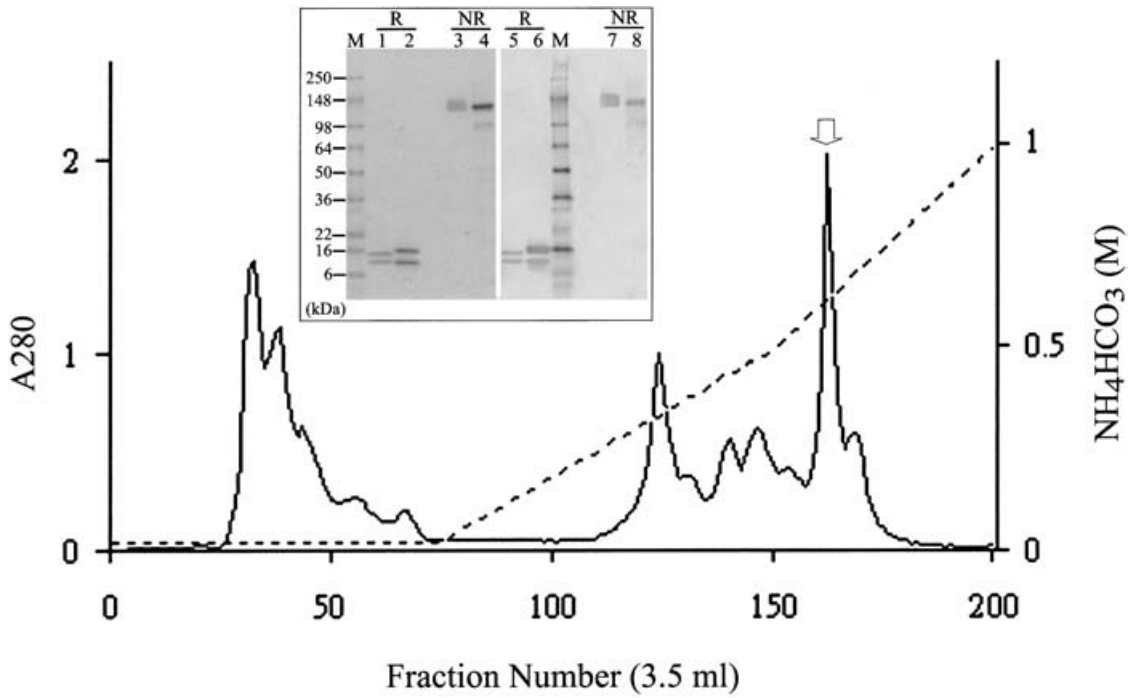


**Figure 1 Isolation of mucrocetin from *T. mucrosquamatus* venom**

Crude *T. mucrosquamatus* venom was separated on a TSK DEAE-650 anion-exchange column by a two-step linear gradient of ammonium bicarbonate. The eluates that contain mucrocetins (indicated with an arrow) were then subjected to purification by successive gel-filtration chromatography as described in the Materials and methods section. Purified proteins were checked on SDS/PAGE (lanes 1–4, inset), or blotted on to PVDF membrane for immunological analysis using an antiserum raised against the $\alpha$-subunit of mucrocetin (lanes 5–8, inset). Inset: lanes 2, 4, 6 and 8 were loaded with mucrocetin, and lanes 1, 3, 5 and 7 were samples of purified FL-A. M, the pre-stained protein markers with molecular masses as indicated in kDa); R, reduced; NR, non-reduced.

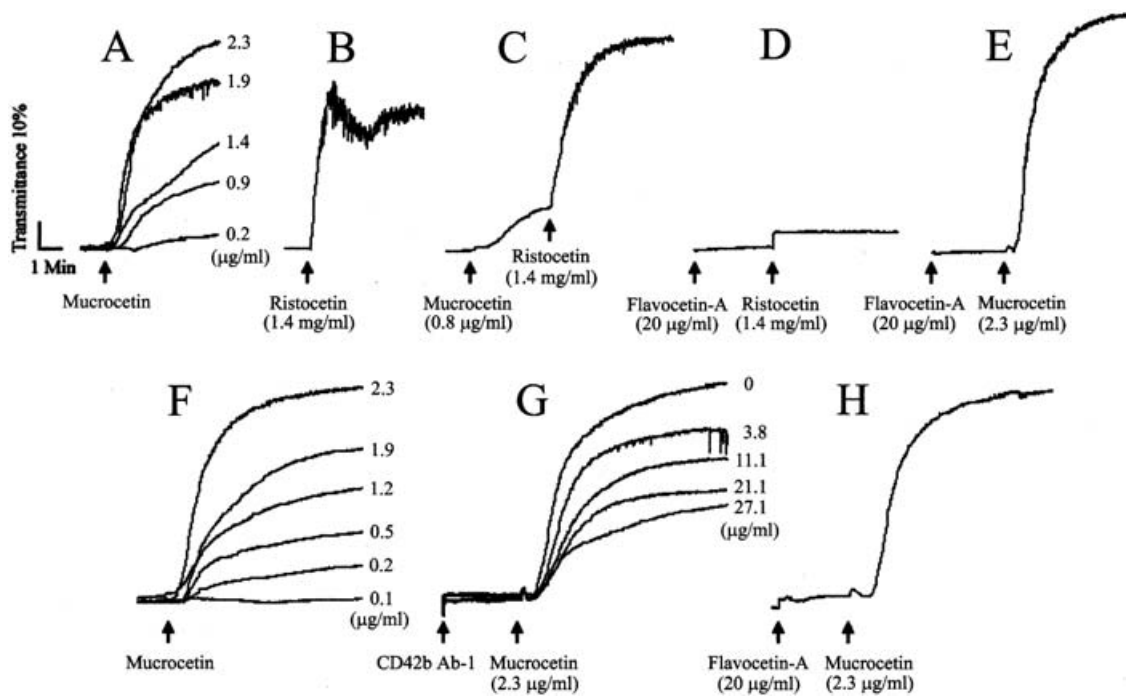


**Figure 2 Platelet-agglutination studies**

Platelet-agglutination assays were carried out in either human PRP (**A**)–(**E**) or washed platelet suspensions (**F**)–(**H**). (**A**) Platelet agglutination was initiated by the addition of various concentrations of mucrocetin as indicated. (**B**) Platelet aggregation was triggered by the addition of the platelet inducer ristocetin. (**C**) Ristocetin was added 3 min after addition of mucrocetin. (**D**) and (**E**) Platelets were pre-incubated with FL-A for 3 min, and then ristocetin and mucrocetin were added respectively. (**F**) Typical patterns of platelet agglutination caused by various concentrations of mucrocetin in washed platelet suspensions. (**G**) Washed platelets were pre-incubated with various concentrations of the anti-GPIb mAb CD42b Ab-1, as indicated, for 3 min, and subsequently mucrocetin was added to trigger platelet agglutination. (**H**) At 3 min after the addition of FL-A, mucrocetin was added to the washed platelet suspension. All of these agglutination responses were continuously monitored by turbidimetry and expressed as an increase in light transmission. Results are representative of duplicate experiments.

HPLC column as described in the Materials and methods section. The N-terminal 20- and 26-amino-acid sequences of the two S-pyridylethylated subunits of mucrocetin were determined by Edman degradation. The larger subunit, designated as $\alpha$, has 25 of its N-terminal 26 residues identical with the $\alpha$-chain of FL-A [14], whereas the smaller one, designated as $\beta$, is the same as the $\beta$-chain of FL-A in their N-terminal 20 residues. In addition, the N-terminal sequences of mucrocetin $\alpha$ and $\beta$ subunits are also identical with those of TMVA [25], a platelet-aggregating factor isolated from the venoms of geographically remote *T. mucrosquamatus*.

### cDNA cloning of mucrocetin

The cDNA encoding the mucrocetin $\alpha$-subunit has a nucleotide sequence of 531 bp, which contains the 5′-untranslated primer region of 24 bp, an open reading frame of 474 bp, a stop codon and the 3′-primer-containing region of 30 bp (GenBank® accession number AY390533). In addition, the cDNA for the nucleotide sequence of $\beta$-subunit is 507 bp, containing the 5′-primer region of 24 bp, an open reading frame of 444 bp, a stop codon and the 3′-primer-containing region of 36 bp (GenBank® accession number AY390534). The deduced amino-acid sequences of the $\alpha$- and $\beta$-subunits of mucrocetin revealed a signal peptide of 23 amino-acid residues, followed by mature subunits of 135 and 125 residues respectively. The predicted N-terminal sequences of $\alpha$- and $\beta$-subunits of mucrocetin are consistent with those by Edman degradation. The calculated molecular masses of $\alpha$- and $\beta$-subunits of mucrocetin are 15729 Da and 14542 Da respectively.

### Sequence comparisons

Comparison of the deduced sequences of mature $\alpha$ and $\beta$ subunits of mucrocetin showed 39.2 % identity, whereas the signal peptides of these two subunits are highly similar to each other (95.7 % identity). The sequence of $\alpha$- and $\beta$-subunits of mucrocetin have 130 out of 135 and 116 out of 125 amino-acid residues identical with those of FL-A respectively (Figure 3). Overall, other GPIb-targeting venom proteins were found to have 46.9–63.5 % sequence identity. The $\alpha$- and $\beta$-subunits of mucrocetin bear higher structural similarity to the $\beta$- and $\gamma$-chains of alboaggregin A (60.7 % and 71.2 % respectively).

### Crystal structure determination

In the refined model, deviations from ideal values of bond lengths and angles are within acceptable range. Most (97.3 %) amino-acid residues have their ($\Phi$, $\psi$) angles in the allowed regions in the Ramachandran plot [26]. $Asp^{\alpha 12}$ ($Asp^{12}$ in $\alpha$-subunit) and $Asp^{\beta 12}$, with ($\Phi$, $\psi$) of about (60, $-110$), occur in a special glycine-like type II $\beta$-turn [27]. Another glycine-like conformation occurs at $Ala^{\alpha 88}$, with ($\Phi$, $\psi$) of (85, $-30$), probably caused by two hydrogen bonds. The disulphide bonds between the cysteine residues $\alpha 4$–$\alpha 15$, $\alpha 32$–$\alpha 129$, $\alpha 81$–$\beta 77$, $\alpha 104$–$\beta 121$, $\beta 4$–$\beta 15$, $\beta 32$–$\beta 121$ and $\beta 98$–$\beta 113$, as well as the interdimer link of $\alpha 135$–$\beta 3$, have good geometry, with bond distances of $2.04 \pm 0.01$ Å between the sulphur atoms. The final statistics are listed in Table 2. The use of NCS restraints resulted in a root-mean-square deviation (r.m.s.d.) in co-ordinates of 0.113–0.259 Å for 1042 backbone atoms and 1.025–1.123 Å for 1085 side-chain atoms between the three heterodimers in an asymmetric unit.

### Crystal packing

In the I422 crystal of mucrocetin, the tetramers are organized into six-layered stacks (or rods) about the crystallographic dyad axis, and these rods are arranged in a mosaic pattern. The six tetramers in a rod can be grouped into three pairs. The tetramers are related by crystallographic dyad symmetry in the central pair, and by non-crystallographic dyad axes in the top and bottom pairs. The total surface area of each mucrocetin tetramer is approx. 48000 Å$^2$, while the interface between the tetramers within a pair buries about 3200 Å$^2$ areas (80 residues) on each tetramer. In addition, there are two types of contacts between the six-layered rod-like stacks of tetrameric molecules in the mucrocetin crystal. The first type occurs between the molecules related by unit-cell translations in the *a*–*b* plane. In other words, each stack is in

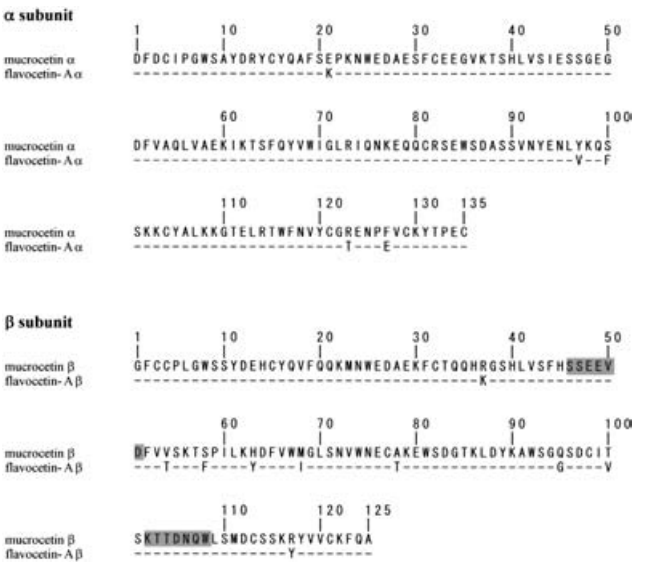


**Figure 3 Sequence comparison of mucrocetin with FL-A**

Identical residues in FL-A are denoted by dashes. The two hydrophilic patches previously observed in the structure of FL-A [14], which are proposed to be involved in GPIb binding, are shaded.

**Table 2 Crystallographic statistics of mucrocetin**

| Parameter | Value |
|---|---|
| Data collection | |
| Space group | I422 |
| Unit cell dimension (Å) | $a = b = 119.9$, $c = 360.8$ |
| Resolution range (Å) | 20–2.8 (2.9–2.8)* |
| Number of observations | 127650 (12356) |
| Unique reflections | 30509 (2971) |
| Completeness (%) | 92.9 (92.3) |
| Average I/$\sigma$(I) | 11.5 (2.9) |
| $R_{merge}$ (%) | 10.0 (48.2) |
| Refinement | |
| Resolution range (Å) | 18–2.8 |
| $R$-factor for 95 % working data set [$> 0\ \sigma(F)$] | 0.235 |
| $R_{free}$ for 5 % test data set | 0.294 |
| R.m.s.d. from ideal bond lengths (Å) | 0.012 |
| R.m.s.d. from ideal bond angles (°) | 1.68 |
| Ramachandran plot: Number of non-proline and non-glycine residues | |
| In most favoured regions (%) | 77.3 |
| In additional allowed regions (%) | 20.0 |
| Average B-value for 6381 protein atoms (Å$^2$) | 52.2 |
| For 601 water molecules (Å$^2$) | 47.9 |

* Numbers in parentheses are for the highest resolution shells.

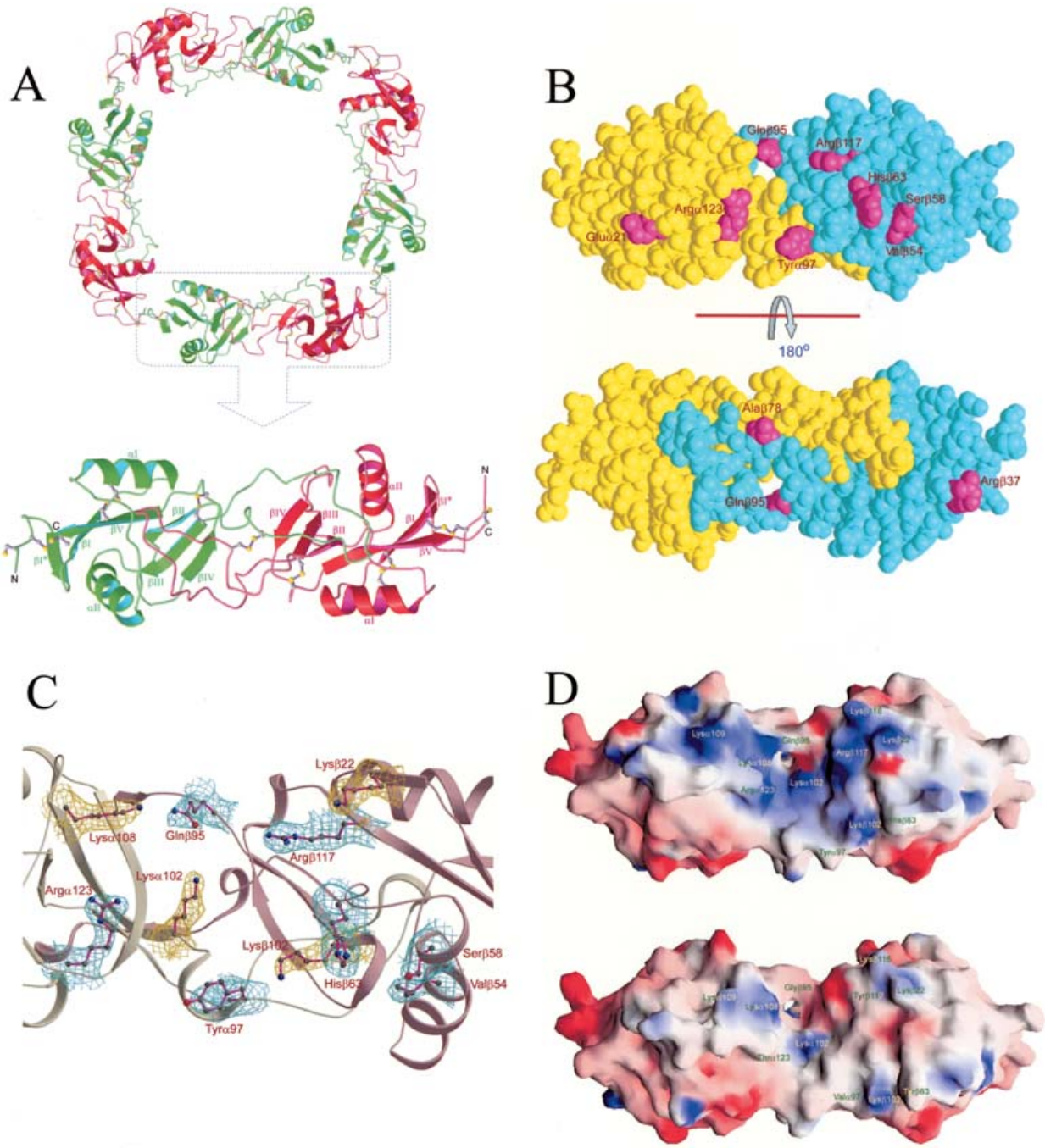


**Figure 4 Overall structure of mucrocetin and the concave binding surface on the molecule**

(**A**) Four heterodimers of the mucrocetin $\alpha$ (red) and $\beta$ (green) subunits are arranged about a 4-fold axis as shown with a ribbon diagram. Within a dimer (lower panel), the two subunits are associated by swapping of the loop domains and an intersubunit disulphide bridge, shown as ball-and-stick models. There are three other disulphide bonds within each subunit. The heterodimers are connected further by intermolecular, 'head-to-tail', disulphide bonds to form a circular tetramer. (**B**) The space-filling model of mucrocetin molecule denotes the substituted residues (pink) on the surface of mucrocetin as compared with those in FL-A. The mucrocetin $\alpha$- and $\beta$-subunits are yellow and cyan respectively. (**C**) The $2F_o$-$F_c$ maps (contoured at the 1.0$\sigma$ level) of mucrocetin around some residues located at the concave binding surface are presented. The density maps for the substituted residues are drawn in light blue and those for the lysine residues that contribute to the positive charges of the binding surface are shown in olive green. (**D**) Diagrams of the surface-charge potential on the mucrocetin (upper) and FL-A (lower) molecules are shown. The surfaces are drawn in red, white and blue for negative, neutral and positive charges respectively. The views are facing the concave binding surface on these two molecules.

'lateral' contacts with four neighbours. The second type occurs between the molecules related by the body-centring translation. Each stack is in 'top–bottom' contacts with eight neighbours. All of the intertetramer contacts comprise hydrogen bonds and salt bridges with no obvious hydrophobic interactions.

## The overall structure of mucrocetin and the comparison with FL-A

The overall structure of mucrocetin, made up of four $\alpha\beta$ heterodimers, is arranged in a square-shaped ring (Figure 4A). This tetrameric ring is stabilized by four interdimer 'head-to-tail'

disulphide linkages of $Cys^{\alpha 135}$–$Cys^{\beta 3}$ between neighbouring heterodimers. The ring has a dimension of approx. $122 \times 122 \times 36$ Å$^3$, delimiting a large central pore of approx. $65 \times 65 \times 36$ Å$^3$. Both the two ($\alpha\beta$) subunits in each heterodimer comprise a globular body and an extending loop. The body is composed of five major $\beta$-strands and two $\alpha$-helices and the loop contributes to dimerization with another subunit. An interdomain disulphide bond between $Cys^{\alpha 81}$ and $Cys^{\beta 77}$ links the swapped loops within each dimer.

The swapped loops are associated with the countersubunit through an extensive contact interface, which buries 1770 Å$^2$ and 1890 Å$^2$ of the 8400 Å$^2$ and 8100 Å$^2$ total surface areas of $\alpha$- and $\beta$-subunits and involves 36 and 35 amino-acid residues respectively. Besides the disulphide bond ($Cys^{\alpha 81}$–$Cys^{\beta 77}$), there are at least 25 direct hydrogen bonds and 12 van der Waals contacts between the two subunits. Interestingly, the segments of residues $\alpha 71$–$\alpha 75$ and $\beta 78$–$\beta 82$ formed an intermolecular anti-parallel $\beta$-like structure. Presumably, this structure and a number of other backbone hydrogen bonds formed in the loop region should contribute to stability of the heterodimer. In contrast, interactions between neighbouring heterodimers in the tetrameric mucrocetin are fewer. The interface buries only 400 Å$^2$ surface areas and involves eight residues on each heterodimer. In addition to the disulphide bond ($Cys^{\alpha 135}$–$Cys^{\beta 3}$), only five hydrogen bonds, but no van der Waals interactions, were observed.

As shown in Figure 3, the amino-acid sequences of mucrocetin and FL-A have the same lengths of 135 and 125 for $\alpha$- and $\beta$-subunits respectively, and they differ only in five and nine residues. The three cyclic tetramers in the crystal structure of mucrocetin can be superimposed on the tetramer of FL-A, with r.m.s.d. of 1.149–1.266 Å for 1040 pairs of C$\alpha$ atoms. If the heterodimers are superimposed individually, the r.m.s.d. are 0.709–0.824 Å for 260 pairs of C$\alpha$ atoms. The results appear to be not very different in all three cases. Mucrocetin does not contain bound calcium ions, whereas the two positively charged lysine residues, $Lys^{\alpha 130}$ and $Lys^{\beta 122}$, substituting for the cations in the binding sites, as in FL-A [14], are conserved. The surface potential diagrams of mucrocetin and FL-A show that the former seems to have more negative charges on the molecule, but the theoretical net charges of the two molecules differ by only one unit at neutral pH.

Ten of the 14 different residues compared with FL-A in mucrocetin are located on the surface of the molecule (see Figure 4B). Although three residues are far away from others, $Tyr^{\alpha 97}$, $Arg^{\alpha 123}$, $Val^{\beta 54}$, $Ser^{\beta 58}$, $His^{\beta 63}$, $Gln^{\beta 95}$ and $Arg^{\beta 117}$ are in the vicinity of the concave binding surface and the positions of their side chains are close (Figure 4C). No obvious conformational changes are observed around the regions with residue substitutions. The concave surfaces of the mucrocetin molecule are facing outside and are not hindered from binding to effector molecules. Surface-charge comparison of the corresponding region in mucrocetin and FL-A shows a significant difference of charge distribution (Figure 4D). In contrast with the structure of FL-A, the side chains of lysine residues at $\alpha 102$, $\alpha 108$, $\alpha 109$, $\beta 22$, $\beta 102$ and $\beta 116$ in mucrocetin tend to point to solvents (Figure 4C). Combined with $Arg^{\alpha 123}$ and $Arg^{\beta 117}$, they form a unique positively charged patch on the binding surface of mucrocetin (Figure 4D).

## DISCUSSION

Binding of plasma vWf to the platelet membrane GPIb–IX–V complex, with exposure to pathological shear stress (e.g. stenosed arteries), is an important event in triggering thrombosis in embolic stroke and cardiovascular disease [28]. This binding process can be modified by several exogenous modulators, including the C-type lectin-like venom proteins. To date, a number of GPIb-BPs have been isolated from the venoms of crotalid and viperid snakes (Table 1). These venom factors serve as useful tools in probing the mechanism of platelet activation and developing a new class of anti-thrombotic agents.

In the present paper, we present a GPIb-BP, mucrocetin, isolated from the venom of Taiwan habu (*T. mucrosquamatus*). Mucrocetin has a structural organization almost identical with those of FL-A and convulxin [14,29]. The molecular mass of mucrocetin calculated from its amino-acid sequence is 121.1 kDa, smaller than those observed on SDS/PAGE (approx. 135 kDa) and gel-permeation chromatography (150–200 kDa), indicating a low compactness in mucrocetin molecules. This is in agreement with the crystal structure of mucrocetin, i.e. a square flat ring with a large central pore. Mucrocetin eluted from the anion-exchange column in the last fractions during the initial isolation step may reflect its acidic property. It is consistent with the observed negative charges on the surface of mucrocetin molecules.

The predicted amino-acid sequence of mucrocetin was confirmed by protein N-terminal sequencing, and the complete sequence is also consistent with its crystal structure, including the distinct residues between mucrocetin and FL-A and those on the concave binding surface. Sequence alignment and comparison of mucrocetin subunits with those of other snake venom GPIb-BPs show various degrees of identity from 38.5 % to 60.7 % in $\alpha$-subunits and 52.0 % to 71.2 % in $\beta$-subunits with 24 and 30 identical residues respectively, suggesting that the $\beta$-subunits are more conserved among these lectin-like venom proteins. Kawasaki et al. [11] proposed that the GPIb-binding site of venom GPIb-BPs resides on the $\beta$-subunit, but not the $\alpha$-subunit. As shown in the structures of mucrocetin and FL-A, the additional $Cys^{135}$ and $Cys^{3}$ in the $\alpha$- and $\beta$-subunit respectively, form an interdimer 'head-to-tail' disulphide linkage. Thus, according to the sequence alignment [30], agglucetin probably possesses a similar interdimer disulphide bridge as well. Nevertheless, these two cysteine residues are not found in the sequence of alboaggregin A [15], in spite of its oligomeric feature.

Mucrocetin dose-dependently induced platelet agglutinations on both PRP and washed platelets with similar turbidimetric profiles, indicating that vWf is not needed on the action of mucrocetin, distinguishable from what was observed on botrocetin and bitiscetin [4,5]. The inhibition studies, using FL-A and an anti-GPIb mAb on mucrocetin-induced platelet agglutination, suggest that mucrocetin is a GPIb agonist with a binding site distinct from that of FL-A on GPIb$\alpha$. In addition, pre-treatment of PRP with mucrocetin showed no effect on the platelet aggregation when stimulated with ristocetin, whereas agglucetin, in a similar experiment performed by Wang and Huang [16], appeared to prevent such a ristocetin-induced aggregation markedly.

The crystal structure of mucrocetin shows a unique crystal packing of six-layer cylinders of doughnut-shaped molecules. The overall structure of mucrocetin is almost identical with the structures of FL-A and convulxin [14,29], with the $\alpha\beta$-heterodimer exhibiting the typical backbone fold of CRD of C-type lectins [31]. The swapped loops in the $\alpha\beta$ heterodimer, which are well conserved among the venom GPIb-BPs, are associated with the globular body of the adjacent subunit. The resulting contact interface, corresponding to the C-interface defined in three-dimensional domain swapping [32], buries approx. 22.4 % of the total surface area of one $\alpha\beta$ heterodimer, and is therefore crucial in connecting the two subunits of mucrocetin. The interface between the $\alpha\beta$ heterodimers is stabilized mainly by interchain disulphide bridges, with only a few non-covalent interactions.

The distinct behaviour of lectin-like venom proteins in recognizing different target molecules, such as coagulation factors, vWf and platelet GPIb, is thought to be in part due to the large

hinge-like motions at the bases of each swapped loop [19]. Only small movements occur when the venom proteins target similar molecules. Consistently, the backbone chain of mucrocetin superimposes well with that of FL-A, and the relative orientations of the $\alpha$- and $\beta$-subunits of these two proteins are almost identical. The structure of the bitiscetin–vWf A1 complex reported by Maita et al. [33] suggested that a positively charged patch on the $\alpha$-subunit of bitiscetin may interact with the C-terminal anionic region of GPIb$\alpha$. However, this basic patch of bitiscetin was not observed in the structures of mucrocetin and FL-A. In addition, two hydrophilic patches were observed in the structure of FL-A $\beta$-subunit [14], which are considered as possible candidates for the platelet GPIb-binding sites. In the structure of mucrocetin, these two peptide fragments were shown to exist as well (Figure 3). The central part of the concave surface in mucrocetin appears to bear more concentrated positive charges than that of FL-A (Figure 4D), although the overall negative charges of mucrocetin structure are slightly greater. Thus, based on these observations, the disparate platelet effects between mucrocetin and FL-A are likely to be the consequence of different charge distributions on the putative binding surface. Namely, the unique positively charged patch formed by several lysine and arginine residues on mucrocetin appears to be the primary determinant of the platelet-agglutinating activity of mucrocetin.

The crystal structures of platelet GPIb$\alpha$ and its complexes with vWf A1 domain or thrombin have been published [34–36]. Three negatively charged patches on the surface of GPIb$\alpha$ were localized to regions that interact with vWf A1 domain and the exosites I and II of thrombin respectively. The interacting surfaces between GPIb$\alpha$ and its bound ligands show the heterogeneous charge distributions and reflect striking charge complementarities. These acidic patches on GPIb$\alpha$ may be the candidates of mucrocetin-targeting site. More structural studies of mucrocetin in complex with GPIb$\alpha$ are needed to elucidate the proposed interaction mechanism.

This work was supported by grants from Academia Sinica (A.H.-J.W.) and National Science Council (S.-H.C.). We are grateful to Dr Jeu-Ming P. Yuann and Dr Yuh-Ling Chen of the Institute of Biological Chemistry at Academia Sinica for kindly providing fresh whole blood and helpful discussion on platelet-agglutination assay respectively. We thank Dr Yuch-Cheng Jean of the National Synchrotron Radiation Research Center (Hsinchu, Taiwan) for assistance in X-ray data collection.

## REFERENCES

1 Roth, G. J. (1991) Developing relationships: arterial platelet adhesion, glycoprotein Ib, and leucine-rich glycoproteins. Blood **77**, 5–19
2 Ruggeri, Z. M. (1999) Structure and function of von Willebrand factor. Thromb. Haemostasis **82**, 576–584
3 Azuma, H., Sugimoto, M., Ruggeri, Z. M. and Ware, J. (1993) A role for von Willebrand factor proline residues 702–704 in ristocetin-mediated binding to platelet glycoprotein Ib. Thromb. Haemostasis **69**, 192–196
4 Fukuda, K., Doggett, T. A., Bankston, L. A., Cruz, M. A., Diacovo, T. G. and Liddington, R. C. (2002) Structural basis of von Willebrand factor activation by the snake toxin botrocetin. Structure **10**, 943–950
5 Matsui, T., Hamako, J., Matsushita, T., Nakayama, T., Fujimura, Y. and Titani, K. (2002) Binding site on human von Willebrand factor of bitiscetin, a snake venom-derived platelet aggregation inducer. Biochemistry **41**, 7939–7946
6 Fujimura, Y., Kawasaki, T. and Titani, K. (1996) Snake venom proteins modulating the interaction between von Willebrand factor and platelet glycoprotein Ib. Thromb. Haemostasis **76**, 633–639
7 Andrews, R. K. and Berndt, M. C. (2000) Snake venom modulators of platelet adhesion receptors and their ligands. Toxicon **38**, 775–791
8 Polgar, J., Magnenat, E. M., Peitsch, M. C., Wells, T. N., Saqi, M. S. and Clemetson, K. J. (1997) Amino acid sequence of the $\alpha$ subunit and computer modelling of the $\alpha$ and $\beta$ subunits of echicetin from the venom of *Echis carinatus* (saw-scaled viper). Biochem. J. **323**, 533–537
9 Chen, Y. L., Tsai, K. W., Chang, T., Hong, T. M. and Tsai, I. H. (2000) Glycoprotein Ib-binding protein from the venom of *Deinagkistrodon acutus*–cDNA sequence, functional characterization, and three-dimensional modeling. Thromb. Haemostasis **83**, 119–126
10 Andrews, R. K., Kroll, M. H., Ward, C. M., Rose, J. W., Scarborough, R. M., Smith, A. I., Lopez, J. A. and Berndt, M. C. (1996) Binding of a novel 50-kilodalton alboaggregin from *Trimeresurus albolabris* and related viper venom proteins to the platelet membrane glycoprotein Ib–IX–V complex: effect on platelet aggregation and glycoprotein Ib-mediated platelet activation. Biochemistry **35**, 12629–12639
11 Kawasaki, T., Fujimura, Y., Usami, Y., Suzuki, M., Miura, S., Sakurai, Y., Makita, K., Taniuchi, Y., Hirano, K. and Titani, K. (1996) Complete amino acid sequence and identification of the platelet glycoprotein Ib-binding site of *jararaca* GPIb-BP, a snake venom protein isolated from *Bothrops jararaca*. J. Biol. Chem. **271**, 10635–10639
12 Sakurai, Y., Fujimura, Y., Kokubo, T., Imamura, K., Kawasaki, T., Handa, M., Suzuki, M., Matsui, T., Titani, K. and Yoshioka, A. (1998) The cDNA cloning and molecular characterization of a snake venom platelet glycoprotein Ib-binding protein, mamushigin, from *Agkistrodon halys blomhoffii* venom. Thromb. Haemostasis **79**, 1199–1207
13 Shin, Y., Okuyama, I., Hasegawa, J. and Morita, T. (2000) Molecular cloning of glycoprotein Ib-binding protein, flavocetin-A, which inhibits platelet aggregation. Thromb. Res. **99**, 239–247
14 Fukuda, K., Mizuno, H., Atoda, H. and Morita, T. (2000) Crystal structure of flavocetin-A, a platelet glycoprotein Ib-binding protein, reveals a novel cyclic tetramer of C-type lectin-like heterodimers. Biochemistry **39**, 1915–1923
15 Kowalska, M. A., Tan, L., Holt, J. C., Peng, M., Karczewski, J., Calvete, J. J. and Niewiarowski, S. (1998) Alboaggregins A and B. Structure and interaction with human platelets. Thromb. Haemostasis **79**, 609–613
16 Wang, W. J. and Huang, T. F. (2001) A novel tetrameric venom protein, agglucetin from *Agkistrodon acutus*, acts as a glycoprotein Ib agonist. Thromb. Haemostasis **86**, 1077–1086
17 Mizuno, H., Fujimoto, Z., Koizumi, M., Kano, H., Atoda, H. and Morita, T. (1997) Structure of coagulation factors IX/X-binding protein, a heterodimer of C-type lectin domains. Nat. Struct. Biol. **4**, 438–441
18 Mizuno, H., Fujimoto, Z., Atoda, H. and Morita, T. (2001) Crystal structure of an anticoagulant protein in complex with the Gla domain of factor X. Proc. Natl. Acad. Sci. U.S.A. **98**, 7230–7234
19 Hirotsu, S., Mizuno, H., Fukuda, K., Qi, M. C., Matsui, T., Hamako, J., Morita, T. and Titani, K. (2001) Crystal structure of bitiscetin, a von Willebrand factor-dependent platelet aggregation inducer. Biochemistry **40**, 13592–13597
20 Huang, K. F., Hung, C. C., Wu, S. H. and Chiou, S. H. (1998) Characterization of three endogenous peptide inhibitors for multiple metalloproteinases with fibrinogenolytic activity from the venom of Taiwan habu (*Trimeresurus mucrosquamatus*). Biochem. Biophys. Res. Commun. **248**, 562–568
21 Taniuchi, Y., Kawasaki, T., Fujimura, Y., Suzuki, M., Titani, K., Sakai, Y., Kaku, S., Hisamichi, N., Satoh, N., Takenaka, T. et al. (1995) Flavocetin-A and -B, two high molecular mass glycoprotein Ib binding proteins with high affinity purified from *Trimeresurus flavoviridis* venom, inhibit platelet aggregation at high shear stress. Biochim. Biophys. Acta **1244**, 331–338
22 Mustard, J. F., Perry, D. W., Ardlie, N. G. and Packham, M. A. (1972) Preparation of suspensions of washed platelets from humans. Br. J. Haematol. **22**, 193–204
23 Otwinowski, Z. and Minor, W. (1997) Processing of X-ray diffraction data collected in oscillation mode. Methods Enzymol. **276**, 307–326
24 Brunger, A. T., Adams, P. D., Clore, G. M., Delano, W. L., Gros, P., Grosse-Kunstleve, R. W., Jiang, J. S., Kuszewski, J., Nilges, M., Pannu, N. S. et al. (1998) Crystallography and NMR system: a new software suite for macromolecular structure determination. Acta Crystallogr. Sect. D Biol. Crystallogr. **54**, 905–921
25 Wei, Q., Lu, Q. M., Jin, Y., Li, R., Wei, J. F., Wang, W. Y. and Xiong, Y. L. (2002) Purification and cloning of a novel C-type lectin-like protein with platelet aggregation activity from *Trimeresurus mucrosquamatus* venom. Toxicon **40**, 1331–1338
26 Laskowski, R. A., MacArthur, M. W., Moss, D. S. and Thronton, J. M. (1993) PROCHECK: a program to check the stereochemical quality of protein structures. J. Appl. Cryst. **26**, 283–291
27 Richardson, J. S. (1981) The anatomy and taxonomy of protein structure. Adv. Protein Chem. **34**, 167–339
28 Ruggeri, Z. M. (2002) Platelets in atherothrombosis. Nat. Med. **8**, 1227–1234
29 Murakami, M. T., Zela, S. P., Gava, L. M., Michelan-Duarte, S., Cintra, A. C. O. and Arni, R. K. (2003) Crystal structure of the platelet activator convulxin, a disulfide-linked $\alpha_4\beta_4$ cyclic tetramer from the venom of *Crotalus durissus terrificus*. Biochem. Biophys. Res. Commun. **310**, 478–482
30 Wang, W. J., Ling, Q. D., Liau, M. Y. and Huang, T. F. (2003) A tetrameric glycoprotein Ib-binding protein, agglucetin, from Formosan pit viper: structure and interaction with human platelets. Thromb. Haemostasis **90**, 465–475

31 Weis, W. I., Kahn, R., Fourme, R., Drickamer, K. and Hendrickson, W. A. (1991) Structure of the calcium-dependent lectin domain from a rat mannose-binding protein determined by MAD phasing. Science **254**, 1608–1615
32 Bennett, M. J., Schlunegger, M. P. and Eisenberg, D. (1995) 3D domain swapping: a mechanism for oligomer assembly. Protein Sci. **4**, 2455–2468
33 Maita, N., Nishio, K., Nishimoto, E., Matsui, T., Shikamoto, Y., Morita, T., Sadler, J. E. and Mizuno, H. (2003) Crystal structure of von Willebrand factor A1 domain complexed with snake venom, bitiscetin: insight into glycoprotein Ib$\alpha$ binding mechanism induced by snake venom proteins. J. Biol. Chem. **278**, 37777–37781
34 Huizinga, E. G., Tsuji, S., Romijn, R. A., Schiphorst, M. E., de Groot, P. G., Sixma, J. J. and Gros, P. (2002) Structures of glycoprotein Ib$\alpha$ and its complex with von Willebrand factor A1 domain. Science **297**, 1176–1179
35 Dumas, J. J., Kumar, R., Seehra, J., Somers, W. S. and Mosyak, L. (2003) Crystal structure of the GpIb$\alpha$–thrombin complex essential for platelet aggregation. Science **301**, 222–226
36 Celikel, R., McClintock, R. A., Roberts, J. R., Mendolicchio, G. L., Ware, J., Varughese, K. I. and Ruggeri, Z. M. (2003) Modulation of $\alpha$-thrombin function by distinct interactions with platelet glycoprotein Ib$\alpha$. Science **301**, 218–221

Received 2 October 2003/10 November 2003; accepted 13 November 2003
Published as BJ Immediate Publication 13 November 2003, DOI 10.1042/BJ20031507